PCCP

PAPER

View Article Online
View Journal

Cite this: DOI: 10.1039/c5cp01305d

High-resolution probing heparan sulfate–antithrombin interaction on a single endothelial cell surface: single-molecule AFM studies†

Cunlan Guo,[a] Xian Fan,[b] Hong Qiu,[b] Wenyuan Xiao,[b] Lianchun Wang[b] and Bingqian Xu*[a]

Received 5th March 2015,
Accepted 13th April 2015

DOI: 10.1039/c5cp01305d

www.rsc.org/pccp

Heparan sulfate (HS) plays diverse functions in multiple biological processes by interacting with a wide range of important protein ligands, such as the key anticoagulant factor, antithrombin (AT). The specific interaction of HS with a protein ligand is determined mainly by the sulfation patterns on the HS chain. Here, we reported the probing single-molecule interaction of AT and HS (both wild type and mutated) expressed on the endothelial cell surface under near-physiological conditions by atomic force microscopy (AFM). Functional AFM imaging revealed the uneven distribution of HS on the endothelial cell surface though they are highly expressed. Force spectroscopy measurements using an AT-functionalized AFM tip revealed that AT interacts with endothelial HS on the cell surface through multiple binding sites. The interaction essentially requires HS to be *N*-, 2-*O*- and/or 6-*O*-sulfated. This work provides a new tool to probe the HS-protein ligand interaction at a single-molecular level on the cell surface to elucidate the functional roles of HS.

Introduction

Heparan sulfate (HS) is a linear polysaccharide ubiquitously expressed in all animal cell plasma membranes.[1] HS consists of alternating *N*-acetylglucosamine (GlcNAc)-uronic acids (iduronic acid, IdoA, or glucuronic acid, GlcA) disaccharide repeating units with various types of sulfation modifications, including *N*-, 2-*O*-, 3-*O*- and 6-*O*-sulflates (*N*S, 2S, 3S and 6S, respectively).[1] The sulfation patterns along the disaccharide repeat units on HS form the unique binding sites for specific protein ligands.[1–3] Such binding between HS and its ligands enables HS to participate in a wide range of biologically important processes from embryonic development and normal physiology (such as blood coagulation and signal transduction) to pathogenesis (such as tumorigenesis and metastasis).[1] To date, the best characterized structure–function relationship of HS in interaction with protein ligands is the specific binding of heparin, a highly sulfated HS, with antithrombin (AT).[4–6] AT, an endogenous anticoagulant, presents abundantly in circulation and inhibits thrombin and other coagulation factors at low activity. Heparin binds AT with high affinity, and critically, the binding induces a conformational change in AT and thereby boosts AT's anticoagulant activity by 2–3 orders of magnitude. The induced enhancement of AT anticoagulant activity underlies the medical application of heparin as a therapeutic anticoagulant and has triggered enormous interest to elucidate the heparin structure that interacts with AT. Previous studies have established that the binding requires a unique pentasaccharide sequence within HS consisting of GlcNAc/NS(6S)-GlcA-GlcNS(3S6S)-IdoA(2S)-GlcNS(6S) (Fig. S1, see ESI†).[6,7] Among the sulfates of the pentasaccharide, the rare 3S of the central *N*-sulfoglucosamine (GlcNS) has been demonstrated to be essential for high affinity AT binding and for the enhancement of AT anticoagulant activity.[8–12] Meanwhile, the removal of NS or 6S was also shown to decrease the binding affinity of AT to heparin.[13,14]

Despite the substantial progress, the exact structure (*i.e.*, sulfation and binding sites) and function (*i.e.*, enhancing anticoagulation) relationship of HS expressed on endothelial cells of the vasculature under physiological conditions remains unclear. Most studies used synthetic heparin mimics or processed heparin, which may not completely reflect the diversity of physiological HS structures.[11–13,15,16] On the other hand, HS is abundantly expressed while no heparin exists in the vasculature.[6] To better understand the structural roles of HS expressed in the vasculature, especially a small percentage of HS containing the pentasaccharide sequence (HS^{AT+}) and thus acting as an AT activator, it is necessary to *in situ* examine its interaction with

[a] *Single Molecule Study Laboratory, College of Engineering and Nanoscale Science and Engineering Center, University of Georgia, Athens, GA, USA. E-mail: bxu@engr.uga.edu; Fax: +1-706-542-3804; Tel: +1-706-542-0502*

[b] *Complex Carbohydrate Research Center and Department of Biochemistry and Molecular Biology, University of Georgia, Athens, GA, USA*

† Electronic supplementary information (ESI) available: Supporting figures. See DOI: 10.1039/c5cp01305d

AT on endothelial cell surfaces. Here we present the first *in situ* single molecule study of HS–AT interaction on a single endothelial cell surface with atomic force microscopy (AFM) to elucidate the critical sulfates that account for AT binding.

AFM offers a mechanistic approach to understand molecular interactions at a single molecular level and provides details for the functions and structures of biomolecular systems.[17–23] It is inherently suitable for high-resolution imaging biomolecules at subnanometer resolution and probing very delicate biological interactions at pico-Newton sensitivity.[21,24–28] Functional AFM imaging and force spectroscopy have been successfully used for investigating DNA, peptides, proteins, cells as well as the interactions of these biological entities with their ligands.[19,24–26,29–32] Though single-molecule interactions of HS with its ligands have been examined with AFM by us and others recently,[21,33] to date no one has been able to probe the single-molecule interactions of endothelial HS with its protein ligands (*e.g.* AT) under near-physiological conditions. This is primarily due to the lack of appropriate endothelial cell models with sulfation-tuneable HS structures.

To address these challenges and to reveal the critical importance of sulfation modification of HS on endothelial cell surfaces in AT binding, in this work we tested with our recently generated mouse lung endothelial cell lines that harbour conditionally targeted HS biosynthetic gene *Ext1* ($Ext1^{f/f}$, wildtype) or *N*-deacetylase/*N*-sulfotransferase-1 ($Ndst1^{f/f}$, wildtype) as well as their corresponding mutant endothelial cell lines $Ext1^{-/-}$ and $Ndst1^{-/-}$ as models.[34,35] Both $Ext1^{f/f}$ and $Ndst1^{f/f}$ endothelial cells express wildtype level HS. In contrast, the $Ext1^{-/-}$ endothelial cells are completely devoid of HS while the $Ndst1^{-/-}$ endothelial cells express undersulfated HS, which bear 50–60% reductions of *N*S, 2S and 6S compared to their "mother" $Ndst1^{f/f}$ endothelial cells.[34,35] Therefore the $Ext1^{-/-}$ and $Ndst1^{-/-}$ cells with their corresponding wildtype control cells provide a unique and informative platform to examine HS and HS structure-dependent AT interaction on the endothelial cell surface as well as the contribution of *N*S, 2S and/or 6S in the HS–AT interactions.

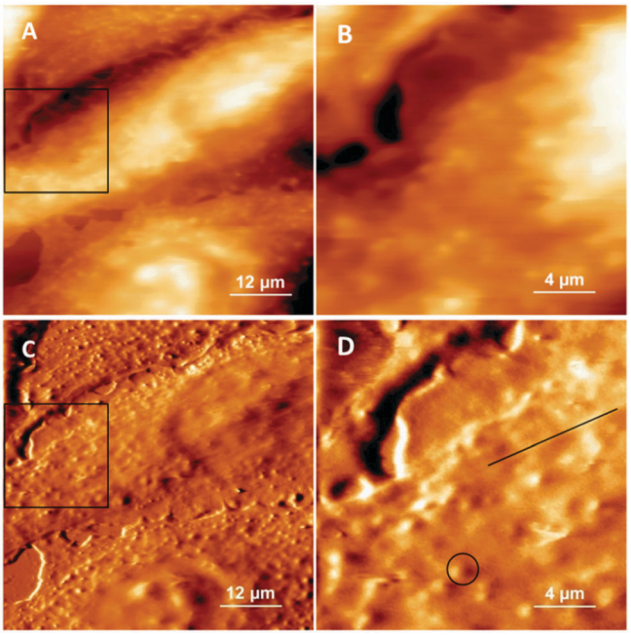

Fig. 1 AFM images of $Ndst1^{f/f}$ cells. (A) Topography images of $Ndst1^{f/f}$ cells. (B) Enlarged area marked with a black square in (A). (C) and (D) are corresponding amplitude images of (A) and (B). Circle and straight line in (D) indicate the features of granule and cytoskeleton on the cell surface, respectively. The images were obtained using Top MAC mode and using a magnetic AFM tip.

Results and discussion

High-resolution AFM imaging endothelial cells

To examine the structural characteristics of endothelial cells under near-physiological conditions, high-resolution AFM imaging was performed on single endothelial cells. AFM can probe mammalian cell morphology under near-physiological conditions without damaging the cells. The AFM image of living cells is usually fuzzy due to the interactions between the tip and the cell membrane that is soft and elastic.[36] In current study, the cells were gently fixed with paraformaldehyde before AFM imaging. This procedure keeps the general features of living cells and meanwhile makes the soft cell surface stiff enough for the access of high resolution in AFM imaging.[31] The endothelial cells were observed by AFM topography imaging, which revealed the structural details of the cell surface at the nanoscale and illustrated the morphology features that are usually blurry under a common optical microscope (Fig. 1). Here, the $Ndst1^{f/f}$ endothelial cells harbouring conditionally targeted *Ndst1* were shown as an example. The cells were oval in shape as the typical morphology of endothelial cells.[31,35] The cell heights varied from approximately 200 nm at the periphery to approximately 1–2.5 μm on the nucleus. The cells displayed a ruffle-like surface. Other distinct features, such as cytoskeletons and granules, were also observed in the topography and amplitude images. Cytoskeletons showed a width at half height ranging from 500 nm to 1.2 μm. Granules, originating from the organelles under the cell membrane, had a width of around 1 μm at half height.

Functional AFM imaging endothelial cells

To further probe the feature and the structure–function relationship of HS on the surface of the endothelial cell membrane, a functional AFM tip that linked a single AT molecule was used to acquire recognition imaging and to perform force measurements. The region of the cell membrane below 1 μm was chosen for the force measurement.

Endothelial cells are one of the major components to form the inner monolayer endothelium in the vasculature and play important roles in homostasis and angiogenesis.[37] HS, abundantly expressed on the endothelial cell surface, is essential to the functions of endothelial cells at both physiological and pathological conditions.[36] HS is biosynthesized as proteoglycans by alternatively adding GlcA and GlcNAc repeating units to core proteins with co-polymerase exostosin (Ext) (Fig. S2, see ESI†).[7] The formed HS backbone is sequentially modified by *N*-deacetylation and *N*-sulfation, *O*-sulfation and epimerization.

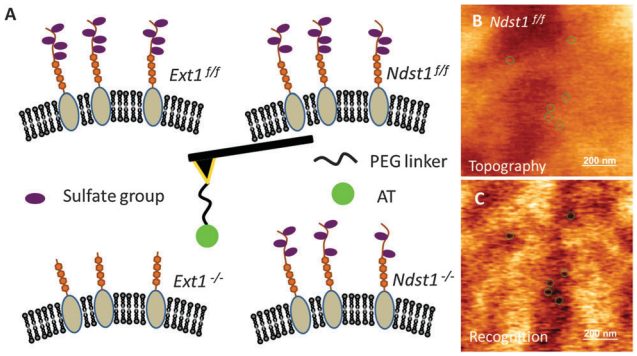

Fig. 2 Functional imaging of the endothelial cell surface using an AT-modified AFM tip. (A) Schematics for cell lines with different levels of HS expression ($Ext1^{f/f}$, $Ext1^{-/-}$, $Ndst1^{f/f}$, and $Ndst1^{-/-}$) as well as an AT-functionalized AFM tip. (B) Topographical image for part of a $Ndst1^{f/f}$ cell surface as an example. (C) The corresponding recognition image of (B).

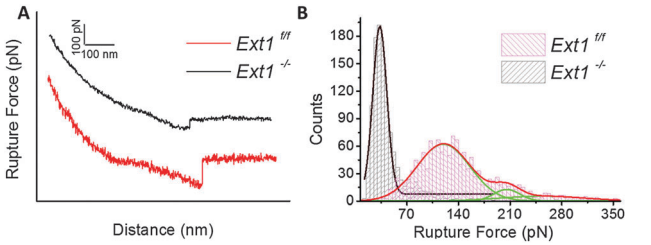

Fig. 3 Force spectroscopy analysis on $Ext1^{f/f}$ and $Ext1^{-/-}$ cell surfaces. (A) representative force–distance curves between an AT-modified tip and HS interaction on $Ext1^{f/f}$ (wildtype) and $Ext1^{-/-}$ endothelial cell surfaces. (B) Comparison of rupture forces between $Ext1^{f/f}$ and $Ext1^{-/-}$ cells. The loading rate is 39 nN s^{-1}, and more than 1000 rupture forces were measured from the force–distance curve for each genotypic cell.

During this process, Ndst catalyzes the *N*-sulfation of GlcNAc units (NS).[37] A recent gene knockout study showed that 3S is essentially required for endothelial HS to bind AT.[6,38] However, the contributions of other sulfation modifications to endothelial HS in interaction with AT remain unclear.[6]

To investigate the function–structure relationship of HS on the endothelial cell surface under near-physiological conditions, we generated endothelial cells with specific knockout of *Ext1* and *Ndst1*, respectively.[35] The endothelial cell identity and HS expression alteration were confirmed by immunofluorescence staining with the anti-PECAM-1 antibody and anti-HS antibody 10E4, respectively (Fig. S3, see ESI†). The resultant mutant cells expressed different levels of HS (Fig. 2A). Compared with $Ext1^{f/f}$ endothelial cells that express the conditionally targeted *Ext1*, the deletion of *Ext1* ($Ext1^{-/-}$) completely diminishes HS expression, while the ablation of *Ndst1* ($Ndst1^{-/-}$) reduces the major sulfation modifications, including *N*-, 2-*O* and 6-*O*-sulfation. By probing the membrane surfaces of these cells with an AT-functionalized AFM tip, the specific AT–HS interaction on the cell surface *in situ* was detected through functional AFM imaging (Fig. 2C). Punctate, dark regions in Fig. 2C indicated the sites where unbinding force was generated between the tip and the cell surface (marked circles in Fig. 2C as examples). The size of the dark regions was between 15 and 30 nm. As AT could strongly bind with the specific sequence of HS (HS^{AT+}), these dark regions therefore represented the range within HS that was the specific binding site for AT and then could be visualized in the recognition image. Moreover, the uneven distribution of the dark regions also suggested that the expression of HS^{AT+} on the cell surface was not uniform though HS was heavily expressed.

Probing HS–AT interactions on endothelial cells by force spectroscopy

The AT–HS binding on cell surfaces was further investigated by force spectroscopy with an AT-functionalized tip (Fig. 3 and 4). For each cell line, more than 5 cells were randomly selected and measured with 2–4 calibrated AT-modified tips. Different cell surfaces gave dramatically different unbinding force profiles. Combined with the knowledge of HS expression levels on different cell surfaces, the unbinding force profiles revealed the information for HS binding sites to AT. As shown in Fig. 3A, the force–distance curves meant single AT–HS unbinding events on both $Ext1^{f/f}$ and $Ext1^{-/-}$ cell surfaces, respectively. Unexpectedly, analysis of rupture force distribution for $Ext1^{f/f}$ cells indicated three maxima at 119.61 ± 35.86 pN, 205.38 ± 17.41 pN, and 253.86 ± 56.64 pN, respectively (Fig. 3B and Fig. S4, ESI†). All of them were significantly stronger than the rupture force from $Ext1^{-/-}$ cells (33.35 ± 11.17 pN) (Fig. 3B), suggesting the specific binding between AT and HS^{AT+} on the $Ext1^{f/f}$ cell surface. The multiple peaks might come from the binding of multiple closely spaced HS with a single AT on the AFM tip or, more likely, from the binding of multiple closely spaced HS to multiple ATs on the AFM tip.[29] However, the force values of peaks 2 and 3 were not exact multiples of the force value of peak 1, indicating that HS may have diverse sites (and diverse saccharide sequences) with different binding affinities for AT. The ratio of these different AT binding affinities was obtained from the analysis of rupture force distribution and is shown in Table 1. On the other hand, since $Ext1^{-/-}$ cells did not express any HS on the cell surface, the obvious decrease of unbinding force for $Ext1^{-/-}$ cells demonstrated that almost no AT–HS interaction occurred between the AT-functionalized tip and the $Ext1^{-/-}$ cell surface. The measured small force of 33.35 pN mainly came from weak nonspecific interaction between the tip and the cell surface.

To further investigate the roles of the major sulfations of endothelial HS, besides the rare 3S sulfation, in AT binding, the force spectroscopy of $Ndst1^{f/f}$ and $Ndst1^{-/-}$ cells was measured using an AT-functionalized tip (Fig. 2A and 4A). Single unbinding events also displayed on both $Ndst1^{f/f}$ and $Ndst1^{-/-}$ cell surfaces, respectively (Fig. 4A). $Ndst1^{f/f}$ cells gave three most probable rupture forces at 59.15 ± 13.43 pN, 92.05 ± 24.20 pN, and 161.72 ± 9.46 pN, which were smaller than the forces for $Ext1^{f/f}$ cells and probably due to the intrinsic difference between the two cell lines. Meanwhile, the rupture force distribution for $Ndst1^{-/-}$ cells indicated a peak at 24.30 ± 7.37 pN (Fig. 4B). Similarly, like $Ext1^{f/f}$ cells, the larger rupture forces obtained from the AT-functionalized tip and the $Ndst1^{f/f}$ cell surface represented the specific binding of AT with HS^{AT+} on the

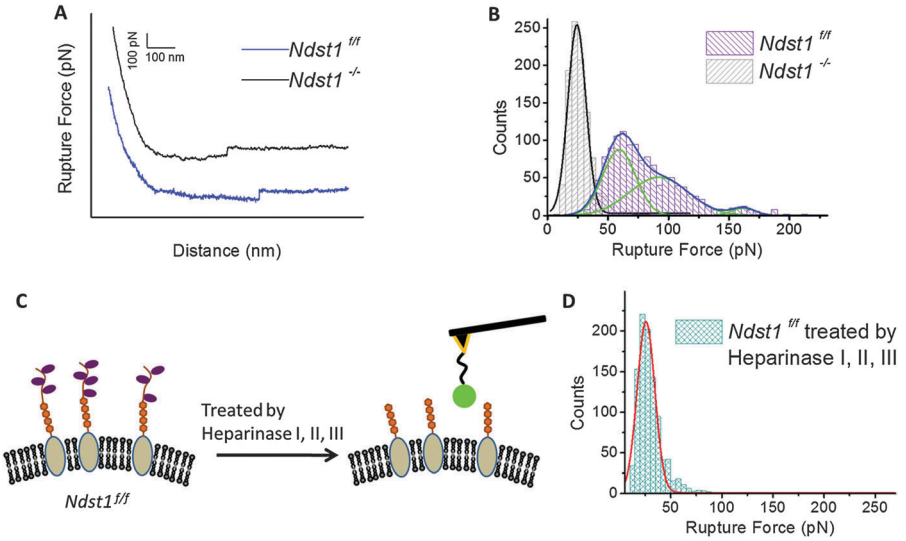

Fig. 4 Force spectroscopy analysis on *Ndst1*$^{f/f}$ and *Ndst1*$^{-/-}$ endothelial cell surfaces. (A) Representative force–distance curves between an AT-modified tip and HS interaction on *Ndst1*$^{f/f}$ and *Ndst1*$^{-/-}$ endothelial cell surfaces. (B) Comparison of rupture forces between *Ndst1*$^{f/f}$ and *Ndst1*$^{-/-}$ cells. (C) Schematic for treatment of *Ndst1*$^{f/f}$ cells with heparinase, and subsequent rupture force determination. (D) Distribution of rupture force after heparinase treatment. The histogram indicates the force decreased to 25.77 ± 8.30 pN. The loading rate was 39 nN s^{-1} and more than 1000 rupture forces were measured from the force–distance curve for each genotypic cell.

Table 1 Rupture force between cell lines *Ext 1* and *Ndst 1*

		Peak 1	Peak 2	Peak 3
Ext1$^{f/f}$	Average force (pN)	119.61 ± 35.86	205.38 ± 17.41	253.86 ± 56.64
	Area distribution (%)	79.55	8.81	1.16
Ext1$^{-/-}$	Average force (pN)	33.35 ± 11.17	—	—
Ndst1$^{f/f}$	Average force (pN)	59.15 ± 13.43	92.05 ± 24.20	161.72 ± 9.46
	Area distribution (%)	46.89	48.60	4.51
Ndst1$^{-/-}$	Average force (pN)	24.30 ± 7.37	—	—

Ndst1$^{f/f}$ cell surface, and multiple rupture force values indicated diverse interactions between AT and different sequences of HS. Since *Ndst1* deletion reduces *N*-, 2-*O* and 6-*O*-sulfation by 50–60%, the dramatically decreased unbinding force indicated that these three major sulfation modifications individually or by their combination are critical for AT–HS^{AT+} binding.

To further confirm the specificity of the rupture force measured from the *Ndst1*$^{f/f}$ surface by an AT-functionalized tip, the *Ndst1*$^{f/f}$ cells were in turn treated by Heparinase I–III before the single molecular force measurement.[39] These enzymes depleted HS expression of *Ndst1*$^{f/f}$ cells (Fig. 4C). After the enzyme treatment, the rupture force between an AT-functionalized tip and the cell membrane surface decreased strikingly to 25.77 ± 8.30 pN (Fig. 4D), which was much close to the rupture force measured from *Ndst1*$^{-/-}$ cells by the same functionalized tip. It confirms that the three rupture forces measured from *Ndst1*$^{f/f}$ cells are specifically related to AT–HS binding on the *Ndst1*$^{f/f}$ cell surface. Meanwhile, the close rupture forces between enzymes treated *Ndst1*$^{f/f}$ cells and *Ndst1*$^{-/-}$ cells also indicated the specificity of the force spectroscopy for AT–HS binding, which may not be easily affected by the environment around the cell surface.

Conclusions

In summary, we elucidated the *in situ* single-molecule interaction of HS with AT on the endothelial cell membrane surface under near-physiological conditions, especially the role of sulfate groups in specific binding sites of HS for AT. With an AT-functionalized AFM tip, force spectroscopy was recorded between AT and the surface of four different cell lines, which expressed HS to different degrees. The functional AFM imaging showed the non-uniform distribution of HS on endothelial cells though they are ubiquitously expressed. The obviously smaller unbinding force from *Ext1*$^{-/-}$ than *Ext1*$^{f/f}$ first confirmed the specific binding of AT and HS on the endothelial cell membrane surface. It also proved that AFM force spectroscopy is suitable for probing single-molecule binding events on intact cells. The different binding events on *Ndst1*$^{f/f}$ and *Ndst1*$^{-/-}$ suggested that major sulfation, that is the *N*S, 2S and 6S individually or their combination, is critical for AT–HS binding on the endothelial cell surface. The anti-HS antibody assay and heparinase treatment assay further validated this conclusion and indicated that the lack of these groups could make HS lose its specific AT binding affinity. Further analysis suggested that wildtype HS expressed in *Ext1*$^{f/f}$ and *Ndst1*$^{f/f}$ cells harbours 3 types of binding

sites for AT. This work provides a new approach to studying the mechanisms of HS related interaction on the cell surface, which are pivotal for understanding the key functions of HS in various biological processes. The established methodology is applicable to other biologically important systems and would facilitate the elucidation of the key functional roles of HS in both physiological and pathological processes.

As mentioned above, in the current report we were not be able to distinguish the role of each individual major sulfate group in HS–AT interaction due to the fact that *Ndst1* deletion reduces *N*S, 2S and 6S simultaneously.[34,41] Meanwhile, whether *Ndst1* deletion alters the 3S level contributing to the reduced AT-binding in endothelial HS remains unknown since we could not detect the 3S-containing disaccharide composition in 3^{H}-glucosamine-labeled endothelial HS which was potentially due to the fact that 3S is very rare and under the detection limitation of disaccharide composition analysis method.[34,38,41] Currently we are in the process of generating new endothelial cell lines that are deficient in 2S, 6S or 3S by ablating their corresponding HS biosynthetic enzyme(s). These newly generated HS mutant endothelial cell lines will allow us to clearly address these unsolved key issues in the near future.

Experimental section

Chemicals and materials

PEG linker (thiol-(polyethylene glycol)-acid, HS-PEG-COOH, M_w 2000) was purchased from Creative PEGWorks. *N*-Hydroxysuccinimide (NHS) and 1-ethyl-3-(3-dimethylaminopropyl) carbodiimide hydrochloride (EDC) were purchased from Sigma-Aldrich. All chemicals were directly used without further purification. AT purified from pooled human plasma was purchased from Athens Research and Technology.

Modify the AFM tip with a PEG linker and AT

Bare silicon (Si) AFM tips (Nanoscience Instruments) were first cleaned and coated with the magnetic material and Au by using an E-beam evaporator. For biochemical modification of the tip, the tip was first immersed in a DMSO solution containing a 0.5 mM HS-PEG-COOH linker and 0.2 mM 1-dodecanethiol for 6 hours. After rinsing with DMSO and water, the carboxyl groups were activated to form *N*-hydroxysuccinimidyl ester by reacting with 10 mM fresh EDC–NHS mixture solution for 30 min. Then the tip was further thoroughly washed with phosphate buffered saline (PBS, pH 7.4) and dipped into AT solution (265 nM, in PBS) overnight. AT was linked on the AFM tip by the reaction between its amino group and *N*-hydroxysuccinimidyl ester. Functionalized tips were stored in PBS before use.

Cell culture and fluorescence imaging

Mouse lung endothelial cell line pairs, including $Ext1^{f/f}$ (wildtype) *vs.* $Ext1^{-/-}$ and $Ndst1^{f/f}$ (wildtype) *vs.* $Ndst1^{-/-}$, were generated as reported in our previous studies.[34,35,40,41] Briefly, we generated immortalized mouse lung endothelial cell lines from conditionally targeted *Ext1* ($Ext1^{f/f}$) and *Ndst1* ($Ndst1^{f/f}$) mice, and subsequently treated the immortalized cell lines with Cre-recombinase and derived corresponding mutant $Ext1^{-/-}$ and $Ndst1^{-/-}$ endothelial cell lines.[34,35,40,41] To verify our test cells are endothelial cells and the $Ext1^{-/-}$ and $Ndst1^{-/-}$ cells are deficient in HS expression, cells were fixed in 4% paraformaldehyde for 10 min at room temperature, washed three times with PBS, and then incubated for 1 hour in blocking buffer (2% goat serum, 0.1% Triton X-100 in PBS). The anti-PECAM-1 antibody (BD Bioscience) or anti-HS antibody 10E4 (Seikagaku Glycoscience) was diluted in blocking buffer at 1 : 100 and applied for 1 h at room temperature or overnight at 4 °C. Secondary antibodies conjugated with FITC (Molecular Probes) were diluted at 1 : 500 in blocking buffer and applied for 1 h at room temperature. Cells were washed twice, permeabilized with 0.5% Triton X-100 in PBS and incubated with cell nuclei dye DAPI (10 μg ml^{-1}) before viewing. Fluorescent images were visualized using a fluorescence microscope (Nikon Eclipse, TE2000-S) with ×20/0.40 and ×40/0.60 objectives at room temperature and captured using a Qimaging (Retiga 1300i Fast) camera and Qcapture version 2.90.1 software. All images were prepared using Photoshop 8.0 (Adobe).

AFM measurement

AFM experiments including imaging and force–distance curve measurement were carried out using an Agilent 5500 AFM system (Agilent, Chandler, AZ). Silicon cantilevers tips with a spring constant of around 0.1 N m^{-1} were used for experiments. Fixed cells were used for AFM measurements. All the images and force–distance curves were obtained in PBS buffer. After imaging, the force–distance curves of AT and HS on the cell surface were measured using an AT-functionalized tip at the loading rate of 39 nN s^{-1}, and more than 1000 rupture forces curves were collected to analyze the force distribution and the most probable rupture force. The region of the cell membrane below 1 μm was chosen for the force measurement. The data analysis was achieved using a homemade LabView computer program.

Acknowledgements

This work was partially supported by U.S. National Science Foundation (Xu: ECCS 1231967 and CBET 1139057) and US National Institute of Health (Wang: R01HL093339 and GM103390).

Notes and references

1 J. R. Bishop, M. Schuksz and J. D. Esko, *Nature*, 2007, **446**, 1030–1037.
2 M. Bernfield, M. Gotte, P. W. Park, O. Reizes, M. L. Fitzgerald, J. Lincecum and M. Zako, *Annu. Rev. Biochem.*, 1999, **68**, 729–777.
3 J. D. Esko and S. B. Selleck, *Annu. Rev. Biochem.*, 2002, **71**, 435–471.
4 P. S. Damus, M. Hicks and R. D. Rosenber, *Nature*, 1973, **246**, 355–357.

5 J. A. Marcum, L. Fritze, S. J. Galli, G. Karp and R. D. Rosenberg, *Am. J. Physiol.*, 1983, **245**, H725–H733.
6 N. W. Shworak, T. Kobayashi, A. de Agostini and N. C. Smits, in *Glycosaminoglycans in Development, Health and Disease*, ed. L. Zhang, 2010, vol. 93, pp. 153–178.
7 M. Petitou, B. Casu and U. Lindahl, *Biochimie*, 2003, **85**, 83–89.
8 Y. M. Xu, C. Cai, K. Chandarajoti, P. H. Hsieh, L. Y. Li, T. Q. Pham, E. M. Sparkenbaugh, J. Z. Sheng, N. S. Key, R. Pawlinski, E. N. Harris, R. J. Linhardt and J. Liu, *Nat. Chem. Biol.*, 2014, **10**, 248–250.
9 U. Lindahl, G. Backstrom, L. Thunberg and I. G. Leder, *Proc. Natl. Acad. Sci. U. S. A.*, 1980, **77**, 6551–6555.
10 L. Roden, in *Heparin*, ed. D. A. Lane and U. Lindahl, Edward Arnold, London, 1989, pp. 1–24.
11 P. Sinay, J. C. Jacquinet, M. Petitou, P. Duchaussoy, I. Lederman, J. Choay and G. Torri, *Carbohydr. Res.*, 1984, **132**, C5–C9.
12 M. Petitou, P. Duchaussoy, I. Lederman, J. Choay, P. Sinay, J. C. Jacquinet and G. Torri, *Carbohydr. Res.*, 1986, **147**, 221–236.
13 C. A. A. Vanboeckel and M. Petitou, *Angew. Chem., Int. Ed. Engl.*, 1993, **32**, 1671–1690.
14 J. Riesenfeld, L. Thunberg, M. Hook and U. Lindahl, *J. Biol. Chem.*, 1981, **256**, 2389–2394.
15 A. Dementiev, M. Petitou, J. M. Herbert and P. G. W. Gettins, *Nat. Struct. Mol. Biol.*, 2004, **11**, 863–867.
16 W. Li, D. J. D. Johnson, C. T. Esmon and J. A. Huntington, *Nat. Struct. Mol. Biol.*, 2004, **11**, 857–862.
17 X. Hao, N. Zhu, T. Gschneidtner, E. O. Jonsson, J. D. Zhang, K. Moth-Poulsen, H. D. Wang, K. S. Thygesen, K. W. Jacobsen, J. Ulstrup and Q. J. Chi, *Nat. Commun.*, 2013, **4**, 2121.
18 P. Zheng, Y. Y. Wang and H. B. Li, *Angew. Chem., Int. Ed.*, 2014, **53**, 14060–14603.
19 D. P. Allison, P. Hinterdorfer and W. H. Han, *Curr. Opin. Biotechnol.*, 2002, **13**, 47–51.
20 M. Kim, C. C. Wang, F. Benedetti and P. E. Marszalek, *Angew. Chem., Int. Ed.*, 2012, **51**, 1903–1906.
21 C. L. Guo, B. Wang, L. C. Wang and B. Q. Xu, *Chem. Commun.*, 2012, **48**, 12222–12224.
22 S. Krysiak, S. Liese, R. R. Netz and T. Hugel, *J. Am. Chem. Soc.*, 2014, **136**, 688–697.
23 Y. Kim, E. S. Kim, Y. Lee, J. H. Kim, B. C. Shim, S. M. Cho, J. S. Lee and J. W. Park, *J. Am. Chem. Soc.*, 2014, **136**, 13754–13760.
24 A. Engel and D. J. Muller, *Nat. Struct. Biol.*, 2000, **7**, 715–718.
25 D. J. Muller and Y. F. Dufrene, *Nat. Nanotechnol.*, 2008, **3**, 261–269.
26 H. D. Wang, L. Obenauer-Kutner, M. Lin, Y. P. Huang, M. J. Grace and S. M. Lindsay, *J. Am. Chem. Soc.*, 2008, **130**, 8154–8155.
27 C. Stroh, H. Wang, R. Bash, B. Ashcroft, J. Nelson, H. Gruber, D. Lohr, S. M. Lindsay and P. Hinterdorfer, *Proc. Natl. Acad. Sci. U. S. A.*, 2004, **101**, 12503–12507.
28 C. M. Lv, X. Gao, W. F. Li, B. Xue, M. Qin, L. Burtnick, H. Zhou, Y. Cao, R. Robinson and W. Wang, *Nat. Commun.*, 2014, **5**, 4623.
29 S. Lee, J. Mandic and K. J. Van Vliet, *Proc. Natl. Acad. Sci. U. S. A.*, 2007, **104**, 9609–9614.
30 D. J. Muller, J. Helenius, D. Alsteens and Y. F. Dufrene, *Nat. Chem. Biol.*, 2009, **5**, 383–390.
31 L. A. Chtcheglova, L. Wildling, J. Waschke, D. Drenckhahn and P. Hinterdorfer, *J. Mol. Recognit.*, 2010, **23**, 589–596.
32 J. J. Valle-Delgado, P. Urban and X. Fernandez-Busquets, *Nanoscale*, 2013, **5**, 3673–3680.
33 S. Block, A. Greinacher, C. A. Helm and M. Delcea, *Soft Matter*, 2014, **10**, 2775–2784.
34 L. C. Wang, M. Fuster, P. Sriramarao and J. D. Esko, *Nat. Immunol.*, 2005, **6**, 902–910.
35 H. Qiu, J. L. Jiang, M. Liu, X. Huang, S. J. Ding and L. C. Wang, *Mol. Cell. Proteomics*, 2013, **12**, 2160–2173.
36 M. M. Fuster, L. C. Wang, J. Castagnola, L. Sikora, K. Reddi, P. H. A. Lee, K. A. Radek, M. Schuksz, J. R. Bishop, R. L. Gallo, P. Sriramarao and J. D. Esko, *J. Cell Biol.*, 2007, **177**, 539–549.
37 R. Sasisekharan and G. Venkataraman, *Curr. Opin. Chem. Biol.*, 2000, **4**, 626–631.
38 S. HajMohammadi, K. Enjyoji, M. Princivalle, P. Christi, M. Lech, D. Beeler, H. Rayburn, J. J. Schwartz, S. Barzegar, A. I. de Agostini, M. J. Post, R. D. Rosenberg and N. W. Shworak, *J. Clin. Invest.*, 2003, **111**, 989–999.
39 L. G. Michelsen, M. Kikura, J. H. Levy, M. K. Lee, K. C. Lee, J. J. Zimmermann and F. Szlam, *Anesthesiology*, 1996, **85**, 339–346.
40 E. Wijelath, M. Namekata, J. Murray, M. Furuyashiki, S. Y. Zhang, D. Coan, M. Wakao, R. B. Harris, Y. Suda, L. C. Wang and M. Sobel, *J. Cell. Biochem.*, 2010, **111**, 461–468.
41 B. Zhang, W. Y. Xiao, H. Qiu, F. M. Zhang, H. A. Moniz, A. Jaworski, E. Condac, G. Gutierrez-Sanchez, C. Heiss, R. D. Clugston, P. Azadi, J. J. Greer, C. Bergmann, K. W. Moremen, D. Li, R. J. Linhardt, J. D. Esko and L. C. Wang, *J. Clin. Invest.*, 2014, **124**, 209–221.

